UC Irvine
UC Irvine Previously Published Works

Title
East Asian summer monsoon variability during Marine Isotope Stage 5 based on speleothem δ18O records from Wanxiang Cave, central China

Permalink
https://escholarship.org/uc/item/6gf8k157

Journal
Palaeogeography Palaeoclimatology Palaeoecology, 236(1-2)

ISSN
0031-0182

Authors
Johnson, Kathleen R
Ingram, B Lynn
Sharp, Warren D
et al.

Publication Date
2006-06-01

DOI
10.1016/j.palaeo.2005.11.041

Peer reviewed

eScholarship.org Powered by the California Digital Library
University of California

Available online at www.sciencedirect.com
SCIENCE DIRECT
ELSEVIER
Palaeogeography, Palaeoclimatology, Palaeoecology 236 (2006) 5–19
PALAEO
www.elsevier.com/locate/palaeo

East Asian summer monsoon variability during Marine Isotope Stage 5 based on speleothem $\delta^{18}O$ records from Wanxiang Cave, central China

Kathleen R. Johnson [a,*], B. Lynn Ingram [a], Warren D. Sharp [b], Pingzhong Zhang [c]

[a] *Department of Earth and Planetary Science, 307 McCone Hall, University of California, Berkeley, CA 94720-4767, USA*
[b] *Berkeley Geochronology Center, 2455 Ridge Rd., Berkeley, CA 94709, USA*
[c] *Center for Arid Environment and Paleoclimate Research (CAEP) and National Laboratory of Western China's Environmental Systems, College of Earth and Environment Sciences, Lanzhou University Lanzhou, Gansu, 730000, China*

Received 30 September 2004; accepted 11 November 2005

Abstract

Speleothems from Wanxiang Cave, China (33°19′ N, 105°00′ E), located near the northern limit of the East Asian summer monsoon, provide high-resolution records of paleomonsoon variability. We present a simple model for interpreting $\delta^{18}O$ shifts in speleothems from this region in which the $\delta^{18}O$ of speleothem calcite is inversely related to monsoon intensity. In contrast to observations at higher latitudes, atmospheric temperature has little effect on $\delta^{18}O$ of precipitation near Wanxiang Cave. Furthermore, the temperature dependence of calcite–water $\delta^{18}O$ fractionation acts in the opposite sense, most likely canceling out the effect of local temperature variations on speleothem $\delta^{18}O$. Given this, the maximum $\delta^{18}O$ shift that could occur due only to changes in the composition of the oceanic source region, the amount of rainfall, and the amount of evaporation between full glacial conditions with a weak summer monsoon and full interglacial conditions with a strong summer monsoon is 5.5‰. Accordingly, it is necessary to invoke changes in past atmospheric circulation patterns and in the ratio of summer to winter precipitation to explain the nearly 7‰ range observed in fossil Wanxiang Cave speleothems. Two stalagmites, WXSM 51 and WXSM 52, exhibit more positive $\delta^{18}O$ during stadial periods (marine isotope stages [MIS] 8, 6, 5d, 5b, and 2) than during interstadial periods (MIS 9, 5a, 5c, 5e). Thus, East Asian summer monsoon intensity is generally decreased during globally cooler periods and increased during globally warmer periods.

We present detailed $\delta^{18}O$ records from MIS 5a–5b and 5c–5d. During the MIS 5d–5c transition, summer monsoon intensity increased steadily from 117.6 ka, with a peak in intensity occurring at 106.8 ka, concurrent with Greenland Interstadial 24. During the MIS 5b–5a transition, monsoon intensity increased abruptly at about 85.7 ka, when $\delta^{18}O$ decreased by approximately 4‰ in 200 years. Monsoon variability, inferred from the MIS 5c–5d and MIS 5a–5b records, closely coincides with global climate changes observed in the GISP2, Vostok, and SPECMAP records, and with the Northern Hemisphere insolation curve. This suggests that East Asian summer monsoon intensity varies in phase with global climate fluctuations and is largely controlled by variations in Northern Hemisphere incident solar radiation. The MIS 5a–5b and 5c–5d paleomonsoon records from Wanxiang Cave also agree well with other records of Asian monsoon variability indicating that $\delta^{18}O$ of speleothems from Wanxiang Cave is a valid proxy for past changes in monsoon intensity.
© 2006 Elsevier B.V. All rights reserved.

Keywords: Asian monsoon; Speleothem; Paleoclimate; MIS 5; Oxygen isotopes

* Corresponding author. Current address: Department of Earth Sciences, University of Oxford, Parks Road, Oxford, OX1 3PR, UK. Fax: +44 1865 272072.
E-mail address: kathleen@earth.ox.ac.uk (K.R. Johnson).

0031-0182/$ - see front matter © 2006 Elsevier B.V. All rights reserved.
doi:10.1016/j.palaeo.2005.11.041

1. Introduction

The East Asian monsoon system, part of the larger Asian–African–Australian monsoon system, is an important part of the global climate system. The intensity of the East Asian monsoon has varied significantly over the past several glacial–interglacial cycles, on a wide range of timescales (10^5 years to intra-annual). On orbital to millennial timescales, the pattern of monsoon variability shows strong similarities to global climate records, indicating that monsoon intensity is controlled primarily by changes in solar radiation and the resulting changes in glacial boundary conditions (Kutzbach and Guetter, 1986; COHMAP, 1988). The higher frequency monsoon variability, on decadal to intra-annual timescales, though less well understood, is largely controlled by ocean–atmosphere–land interactions, such as those related to ENSO (Webster et al., 1998).

The history of the East Asian monsoon has been described by An (2000) as an alternation between the dominance of the dry-cold northwesterly winter monsoon and the warm-humid southeasterly summer monsoon systems. In general, colder stadial periods are characterized by a dominance of the dry winter monsoon, due to the presence of higher Siberian High and Tibetan High pressure systems that lead to increased strength of the mid-latitude westerlies and their migration to lower latitudes. This, in turn, inhibits northward migration of the Intertropical Convergence Zone (ITCZ) and the associated band of heavy summer monsoon precipitation (Kutzbach et al., 1992; Zhou et al., 1999). Conversely, warmer interstadial periods are characterized by dominant summer monsoons, due to the relatively lower high-pressure systems with the westerly barrier to the ITCZ migration positioned farther north.

The natural pattern of monsoon variability, both temporally and spatially, is still not well understood. Even small variations in monsoon intensity can have devastating effects on society in monsoon regions, where there is a strong agricultural dependence on the summer monsoon precipitation (Webster et al., 1998). Successful prediction of monsoon variability, both natural and global-warming related, is crucial to the livelihood of the billions of people living in the Asian monsoon region. Thus, there is a need for high-resolution proxy records of paleomonsoon intensity. To date, the most complete records of East Asian monsoon variability come from the Chinese Loess deposits (Chen et al., 1999; An, 2000; Porter, 2001). Other records of East Asian monsoon variability have been obtained from marine records from the South China Sea (Wang et al., 1999; Sun et al., 2003; Wang et al., 2003), tree ring records (Feng et al., 1999; Feng et al., 2002; Zhou, 2002), Tibetan ice cores (Thompson et al., 1989; Thompson et al., 1997; Thompson et al., 2000), lake records (Gasse et al., 1991; An et al., 2000), and speleothem records (Wang et al., 2001; Zhao et al., 2003; Yuan et al., 2004). Of these proxies, speleothems hold the greatest potential for yielding high-resolution, precisely dated records of summer monsoon variability over the last several glacial–interglacial cycles.

Speleothems are well suited for paleoclimate reconstruction, as they are very pure, well preserved, can be precisely dated using U-series methods, and may contain numerous types of paleoclimate proxy data ($\delta^{18}O$, $\delta^{13}C$, annual layer thickness, δD of fluid inclusions, trace element concentrations, luminescence, etc.) in their highly resolvable growth bands (Gascoyne, 1992; Bar-Matthews et al., 1997; Neff et al., 2001; Fleitmann et al., 2003; Fleitmann et al., 2004). Speleothem $\delta^{18}O$ records of Asian monsoon intensity have been presented for regions in southern China, well within the region dominated by the summer monsoon precipitation (Wang et al., 2001; Zhao et al., 2003; Yuan et al., 2004). We present $\delta^{18}O$ records from two stalagmites from Wanxiang Cave, located farther north, near the northern boundary of the summer monsoon region to assess the potential of speleothems from this region as paleomonsoon archives.

2. Study area

The samples, WXSM 51 and WXSM 52, presented in this study, were collected in Wanxiang Cave (33°19′ N, 105°00′ E), Southern Gansu Province, China. Wanxiang Cave is an active cave with abundant modern and fossil speleothems, located in the Qinling Mountains, a key geographic location on the eastern edge of the Qinghai–Tibetan Plateau and the southwest edge of the Loess Plateau, near the modern northern limit of the summer monsoon precipitation (Fig. 1). The cave is approximately 1100 m long and has only one major entrance, located at an elevation of 1194 m, approximately 300 m above the Bailong River valley floor (Fig. 2). The cave is situated primarily along a single, tilted bedding plane in the Silurian (428 ma) Gongpo Quan Limestone and is overlain by approximately 30 to 250 m of limestone bedrock and approximately 10 m of loess. The environmental conditions in and around Wanxiang Cave were studied in October 1999, September 2001, and May 2002. The temperatures measured in the deepest parts of the cave, where all of the stalagmites

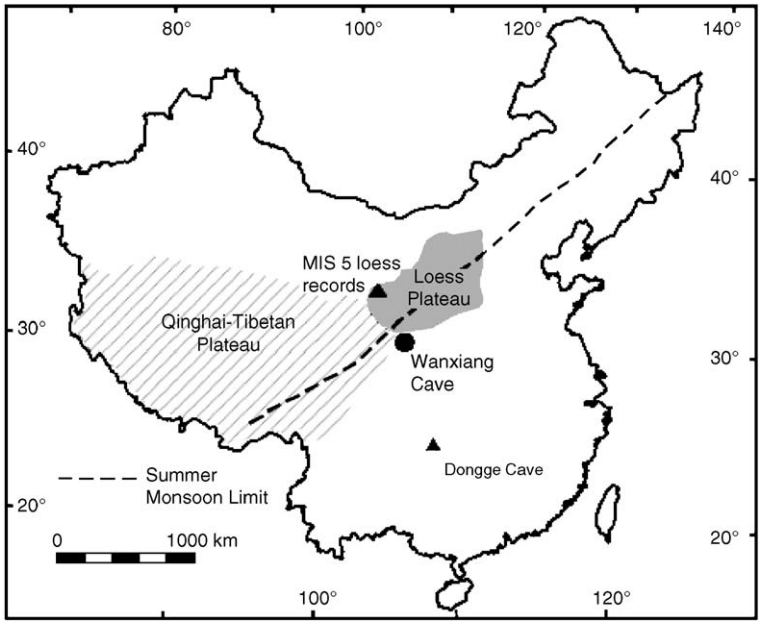

Fig. 1. Map showing the location of Wanxiang Cave relative to the Chinese Loess Plateau, the Qinghai–Tibetan Plateau, and the northern limit of the summer monsoon. The location of Dongge Cave (Yuan et al., 2004) and the loess deposits studied by Chen et al. (1999) are also shown.

were sampled, range from 10.5 to 11.2 °C and remain constant throughout the year. The measured relative humidity in the cave ranges from 95% to 100%. The drip rates are high and range from approximately 10 to 100 drips per min. As typical of monsoon regions, the majority (~75%) of rainfall at Wanxiang Cave occurs

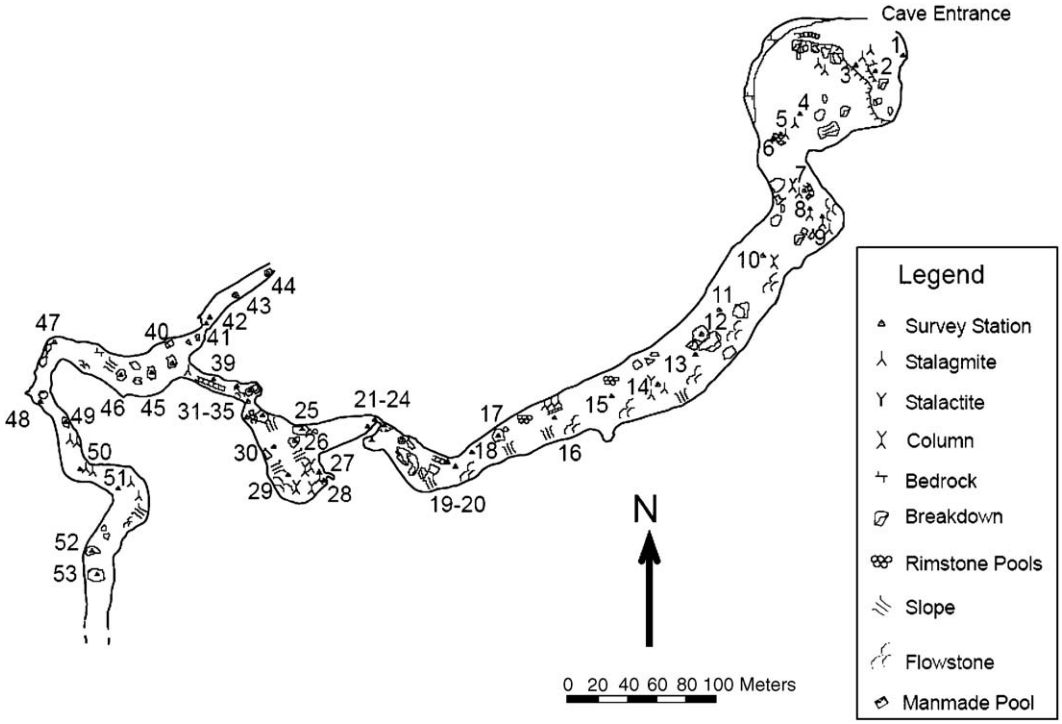

Fig. 2. Survey (plan map) of Wanxiang Cave. The numbered survey stations are the basis of the speleothem sample nomenclature. WXSM 51 and WXSM 52 were collected from near survey stations 51 and 52, respectively.

between the warmest months of May through September. The mean annual temperature (MAT) at Wanxiang Cave is approximately 12.6 °C. The climate at Wanxiang Cave is semi-arid, with a mean annual precipitation (MAP) of approximately 489 mm.

The results of a study of the modern carbonate–water stable isotope systematics in Wanxiang Cave, suggest that speleothems from this site are well suited for paleoclimate reconstructions (Zhang et al., 2004). The isotopic composition of cave drip water is constant throughout the year (mean $\delta^{18}O = -9.08‰$, mean $\delta D = -63.2‰$) and closely reflects the mean annual precipitation in the region ($\delta^{18}O = -9.30‰$, $\delta D = -60.0‰$) as inferred from a nearby spring. In addition, modern speleothem calcite appears to be forming in isotopic equilibrium with the cave drip water. In the deeper parts of the cave, where evaporative effects should be insignificant due to the high relative humidity (100%), isotopic temperatures were calculated using the $\delta^{18}O$ of modern calcite and modern drip water, and the carbonate paleotemperature equation (Epstein et al., 1953; O'Neil, 1969). The calculated isotopic temperatures agree closely (within ~1 °C) with the estimated mean annual temperature and the measured temperatures in the cave, indicating that the system is close to equilibrium.

The results of stable isotope measurements made along individual growth bands are shown in Fig. 3. Hendy (1971) proposed a test for isotopic equilibrium conditions in speleothems in which the $\delta^{18}O$ and $\delta^{13}C$ should be measured along the length of individual growth bands. If the samples had been significantly affected by kinetic fractionation due to rapid CO_2 degassing and/or evaporation, significant variability in $\delta^{18}O$ and a correlation between $\delta^{18}O$ and $\delta^{13}C$ would be observed along individual growth bands. The Hendy criterion (Hendy, 1971) for isotopic equilibrium appears to be satisfied in the fossil speleothem growth bands. Although the Hendy Test is not as robust a test of equilibrium as observing similar isotopic records in separate contemporaneous speleothems, the fact that there is little variation in $\delta^{18}O$ along individual growth bands and that $\delta^{18}O$ and $\delta^{13}C$ are not significantly correlated is consistent with a lack of kinetic fractionation effects. Accordingly, we assume that fossil speleothems collected from Wanxiang Cave formed in isotopic equilibrium with drip water and that $\delta^{18}O$ variations along their growth axes reflect only changes in cave temperature and drip water composition.

3. Sample description

Samples WXSM 51 and WXSM 52, both stalagmites, were collected from the deepest parts of Wanxiang Cave, where temperature, drip water composition, and relative humidity are constant throughout the year. WXSM 51 (Fig. 4) is 402 mm in length, measured

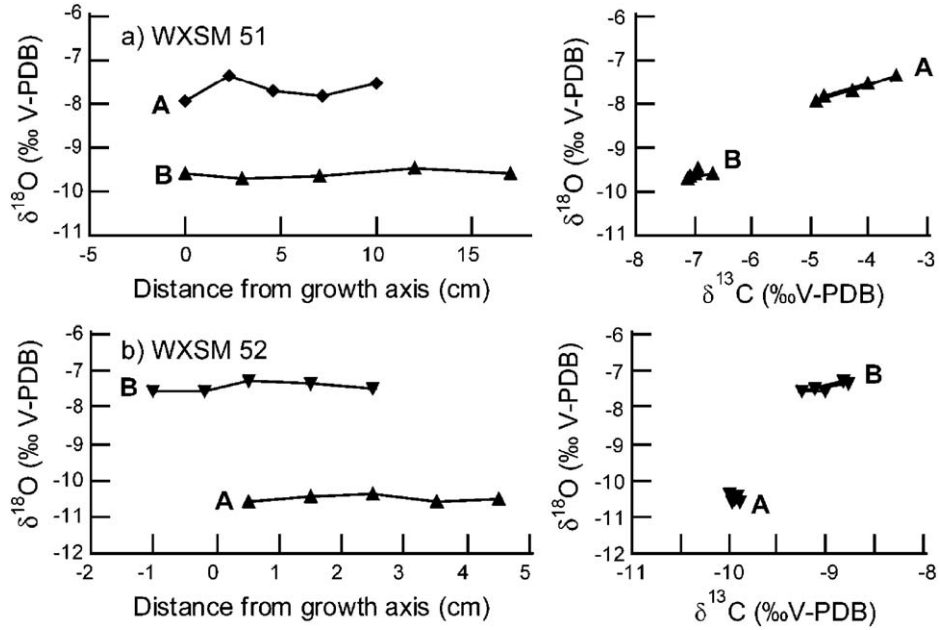

Fig. 3. 'Hendy' tests for 2 growth horizons (A and B) from WXSM 51 (a) and WXSM 52 (b). $\delta^{18}O$ within individual horizons varies by less than 0.5‰, indicating the lack of significant kinetic effects related to evaporation. $\delta^{13}C$ varies by less than 1‰ and is not strongly correlated with $\delta^{18}O$, except for possibly in WXSM 51 band A.

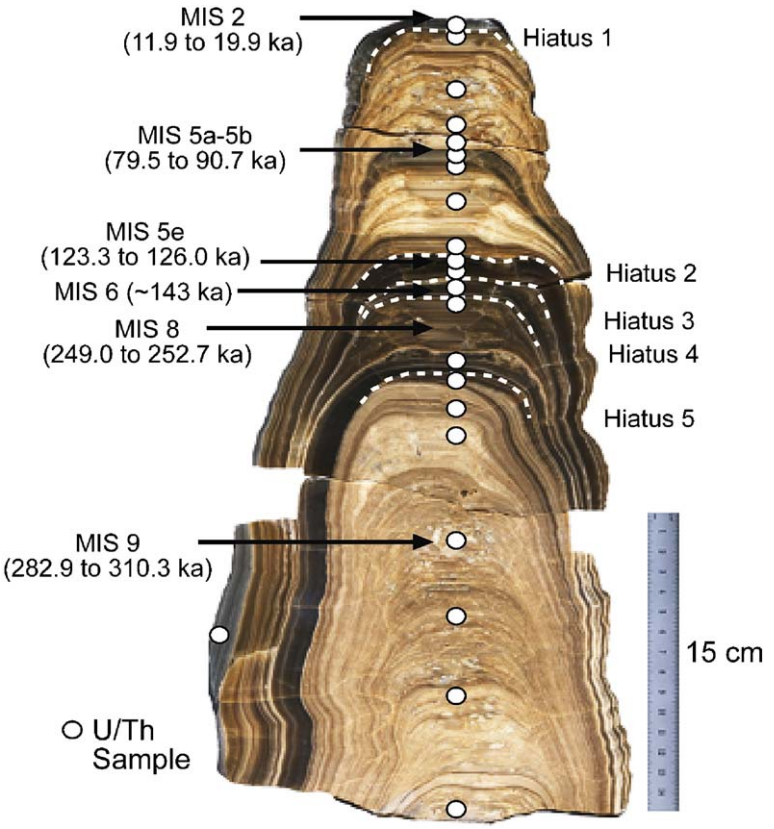

Fig. 4. Scanned image of WXSM 51, showing U–Th sample locations and the location of the major depositional hiatuses. The age range and Marine Isotope Stage (MIS) of calcite deposited between hiatuses is also indicated.

along its primary growth axis, and is punctuated by five major depositional hiatuses, located at 6, 128, 143, 150, and 182 mm from the top. WXSM 52 (Fig. 5) measures 356 mm along its growth axis, and is punctuated by only one major hiatus at 174.5 mm. These hiatuses may reflect a regional environmental change, such as prolonged aridity or permafrost at the surface or simply a local change related to a change in drip location or flooding in the cave. Both samples are composed primarily of coarse, columnar crystals of calcite, oriented parallel to the growth axis. Both speleothems exhibit visible growth banding and color changes throughout, which may be another measure of past environmental conditions.

4. Analytical methods

4.1. U-series dating

Samples for U–Th dating were collected at key points along the speleothem growth axes, including at the top and bottom of each sample, above and below any suspected hiatus, and about every 3–4 cm along speleothem sections characterized by visibly continuous deposition. The 100–200 mg samples were drilled out, parallel to speleothem growth bands, using the 'moat-and-spall' technique, whereby a small trench is drilled around the desired sample region using a 0.5 mm dental drill. The tablet-shaped sample is then broken off at its base, cleaned by ultrasonic washing in isopropanol, and then rinsed in Millipore H_2O. After drying, the samples were weighed and completely dissolved in 7N HNO_3, and a mixed ^{233}U–^{236}U–^{229}Th spike was added. U and Th were separated using conventional ion exchange methods and loaded as a colloidal graphite sandwich onto single rhenium filaments (Chen et al., 1986; Edwards et al., 1987).

The U–Th isotopic analyses were performed on a Micromass Sector-54 thermal ionization mass spectrometer (TIMS) equipped with a high abundance-sensitivity filter and a Daly type ion counter. U mass fractionation was corrected for using the spike $^{233}U/^{236}U$. No correction was applied for Th fractionation. Ages and errors were calculated using Isoplot/Ex

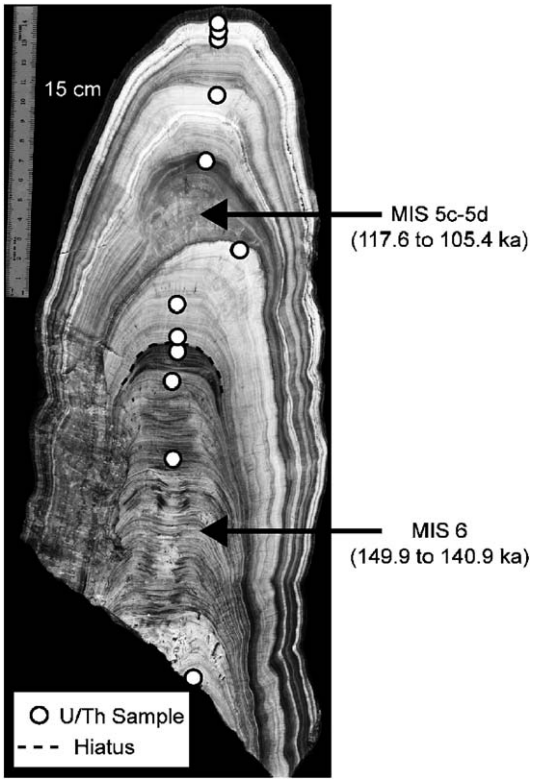

Fig. 5. Scanned image of WXSM 52, showing U–Th sample locations and the location of the depositional hiatus which lasted from 140.9 to 117.6 ka.

(Ludwig, 1999) and the half-lives used are those of Cheng et al. (2000). Corrections for initial isotopes of U and Th from detritus were made by using ^{232}Th as an index isotope, assuming that initial U and Th were derived from crustal silicates with a ^{232}Th/^{238}U = 1.2 ± 0.6, ^{234}U/^{238}U = 1.0 ± 0.1, and ^{230}Th/^{238}U = 1.0 ± 0.1 (Ludwig and Paces, 2002). The resulting age corrections were negligible for the vast majority of samples reported in this study.

4.2. Oxygen isotope analysis

Samples for stable isotope analysis (δ^{18}O and δ^{13}C) were collected from the top 8 cm of WXSM 51 at an average resolution of 0.5 mm using a Merchantek Computer Controlled Micromilling system. The remainder of WXSM 51 was sampled at a resolution of 1–2 mm using a 1 mm dental drill. WXSM 52 was sampled at an average resolution of 0.8 mm along its entire growth axis using a 0.5 mm dental drill. WXSM 51 microsamples were analyzed at UC Davis, where CO_2 for isotopic analysis was produced by reacting 0.01–0.05 mg carbonate with phosphoric acid (Mccrea, 1950) using an Isocarb automated carbonate device attached to a VG Optima mass spectrometer. WXSM 52 microsamples were analyzed at Stanford University, where 60–100 μg samples were reacted with phosphoric acid in a Kiel III carbonate device interfaced with a Finnigan MAT 252 IRMS. Oxygen and carbon isotopic data are reported in the δ notation relative to the VPDB standard for carbonate samples, where $\delta^{18}O = [(R \text{ sample})/(R \text{ std}) - 1] \times 1000$, and $R = {}^{18}O/{}^{16}O$ for oxygen and ^{13}C/^{12}C for carbon. The precision for each analysis is ±0.05‰ for carbon and ±0.06‰ for oxygen.

5. Results

5.1. Uranium-series ages

The TIMS U-series results are shown in Table 1. All reported ratios are activity ratios with 2σ errors given. ^{230}Th/^{232}Th activity ratios are generally high, ranging from 14.9 to > 80,000; thus, detritus corrections are minor or negligible. Twenty-three dated samples from speleothem WXSM 51 range in age from 12 to 321 ka and 13 samples from speleothem WXSM 52 range from 93 to 151 ka. All samples measured are in correct stratigraphic order within errors. The dated speleothems exhibit limited ranges of calculated initial ^{234}U/^{238}U—1.94–2.40 and 1.23–1.48, respectively, for WXSM 51 and WXSM 52, which are consistent with closed system evolution of samples with a limited range of initial ^{234}U/^{238}U.

5.2. Speleothem growth models

WXSM 51 was deposited in 2 extended and 3 short episodes, punctuated by long depositional hiatuses. The growth model (Fig. 6) was constructed using a stepwise linear fit method. Based on this model, the sample began growing during MIS 9, around 310 ka and grew continuously until about 283 ka. Hiatus 5 lasted for the next 30 ka until speleothem growth resumed during MIS 8 at 252 ka. Growth continued until about 249 ka, when Hiatus 4, a 106 ka break in speleothem deposition, began. Growth resumed for short periods during MIS 6 (~143 ka) and MIS 5e (~125 ka), punctuated by Hiatus 3 and 2, respectively. The sample then underwent another extended period of calcite precipitation during MIS 5a and 5b, from about 90 to 79 ka. Hiatus 1 lasted until the Last Glacial Maximum, when speleothem growth occurred between 19.9 and 11.9 ka. The average growth rate for the MIS 5a–5b period is 1 cm/ka and for the MIS 9 period is 8 mm/ka. Thus, the interval between WXSM 51 stable isotope samples is 50–100 years during MIS 5a–5b and 125–250 years during MIS 5c–5d.

Table 1
TIMS U-series dating results[1] from samples WXSM 51 and WXSM 52

Sample name	Distance (mm)	Wt. (mg)	U (ppm)	^{232}Th (ppm)	[^{230}Th / ^{232}Th]	Measured		Detritus-corrected		Age (ka)	Initial [^{234}U/^{238}U]
						[^{230}Th/^{238}U]	[^{234}U/^{238}U]	[^{230}Th /^{238}U]	[^{234}U /^{238}U]		
WXSM 51											
U-51-1	0	205.1	3.6	0.003	814.3	0.218±3.211	2.084±0.220	0.218±3.215	2.084±0.220	12.0±0.4	2.121±0.005
U-51-2	5	203.1	3.2	0.010	345.5	0.349±1.833	2.057±0.410	0.349±1.839	2.058±0.411	20.0±0.4	2.119±0.009
U-51-3	7	199.8	1.7	0.014	390.5	1.023±0.985	1.884±0.200	1.023±0.987	1.886±0.207	79.4±1.1	2.109±0.005
U-51-4	40	145.2	1.4	0.000	11012.4	1.013±0.533	1.839±0.150	1.013±0.533	1.839±0.150	81.3±0.6	2.056±0.003
U-51-5	57	168.6	1.4	0.002	2559.4	0.992±1.274	1.820±0.490	0.992±1.274	1.820±0.490	80.2±1.5	2.029±0.010
U-51-6	61	200.5	1.2	0.010	377.9	1.014±1.633	1.822±0.130	1.014±1.637	1.824±0.140	82.4±1.9	2.040±0.006
U-51-7	64	154.7	1.4	0.001	6485.7	1.022±0.938	1.828±0.340	1.022±0.938	1.828±0.340	83.0±1.2	2.047±0.007
U-51-8	67	76.6	2.8	0.000	18673.3	1.051±1.416	1.841±0.390	1.051±1.416	1.841±0.390	85.5±1.8	2.071±0.009
U-51-9	85	192.4	2.0	0.002	3022.1	1.020±1.585	1.782±0.360	1.020±1.586	1.782±0.360	86.0±2.0	1.998±0.009
U-51-10	123	152.0	1.6	0.000	12310.0	1.074±0.619	1.812±0.210	1.074±0.619	1.812±0.210	90.2±0.9	2.048±0.005
U-51-11	130	109.3	5.7	0.004	6230.2	1.285±0.795	1.775±0.160	1.285±0.795	1.775±0.160	123.3±1.7	2.099±0.006
U-51-12	142	196.1	5.5	0.009	2480.1	1.311±0.454	1.787±0.100	1.311±0.455	1.788±0.101	126.1±1.0	2.125±0.004
U-51-13	144	192.0	7.0	0.006	4813.0	1.466±1.585	1.852±0.100	1.466±1.586	1.852±0.100	143.5±4.2	2.278±0.015
U-51-14	149	104.8	4.0	0.003	6852.6	1.417±1.062	1.796±0.100	1.417±1.062	1.796±0.100	143.2±2.8	2.193±0.010
U-51-15	156	133.3	2.0	0.006	1593.8	1.693±2.312	1.674±0.260	1.694±2.313	1.675±0.261	259.2±19.3	2.404±0.076
U-51-16	181	190.7	4.0	0.000	86187.1	1.624±0.510	1.629±0.570	1.624±0.510	1.629±0.570	251.3±6.5	2.279±0.014
U-51-17	190	159.8	1.6	0.008	922.8	1.605±1.736	1.578±0.180	1.606±1.738	1.579±0.182	272.7±16.6	2.250±0.058
U-51-18	193	200.3	1.5	0.002	4578.3	1.577±0.559	1.534±0.420	1.578±0.559	1.534±0.420	288.9±8.2	2.209±0.021
U-51-19	204	124.0	1.7	0.003	2915.4	1.486±1.336	1.450±0.140	1.486±1.337	1.450±0.140	297.5±16.3	2.043±0.048
U-51-20	277	197.7	1.0	0.002	2176.9	1.456±1.299	1.422±0.480	1.457±1.299	1.422±0.480	301.2±17.9	1.989±0.046
U-51-21	313	207.6	0.9	0.005	908.7	1.432±1.027	1.414±0.220	1.433±1.028	1.415±0.221	289.1±12.1	1.939±0.031
U-51-22	338	200.5	1.0	0.003	1339.5	1.469±1.484	1.416±0.240	1.470±1.485	1.416±0.241	320.9±22.6	2.030±0.065
U-51-23	402	200.9	1.0	0.012	383.7	1.497±0.516	1.441±0.160	1.499±0.520	1.443±0.169	316.1±7.8	2.082±0.023
WXSM 52											
U-52-2	2	157.2	0.3	0.023	35.6	0.844±1.219	1.302±0.350	0.841±1.284	1.308±0.453	106.3±2.4	1.416±0.007
U-52-3	3	119.8	0.3	0.034	25.3	0.865±0.890	1.321±0.360	0.861±1.007	1.330±0.559	107.3±2.1	1.447±0.009
U-52-4	3	126.4	0.7	0.001	2644.3	0.854±0.357	1.309±0.190	0.854±0.357	1.309±0.190	109.0±0.7	1.421±0.003
U-52-6	60	125.9	0.3	0.007	107.0	0.867±1.623	1.358±4.960	0.866±1.638	1.360±4.986	104.0±9.4	1.484±0.079
U-52-7	78	147.2	1.0	0.008	750.8	0.871±0.528	1.310±0.400	0.870±0.530	1.311±0.402	112.1±1.3	1.427±0.006
U-52-9	121	139.9	0.4	0.003	382.0	0.864±0.843	1.290±0.550	0.863±0.845	1.290±0.551	113.9±2.0	1.401±0.009
U-52-10	152	159.0	0.8	0.001	2027.6	0.878±2.226	1.312±0.640	0.878±2.227	1.313±0.640	113.6±4.4	1.431±0.011
U-52-11	173	177.2	0.8	0.002	1192.9	0.896±3.071	1.312±0.320	0.896±3.073	1.312±0.320	117.5±6.2	1.435±0.009
U-52-12	178	191.0	1.2	0.004	771.3	0.878±0.701	1.183±0.290	0.877±0.702	1.183±0.290	139.7±2.1	1.272±0.005
U-52-13	196	188.8	1.0	0.002	1347.0	0.887±1.326	1.155±0.740	0.887±1.327	1.155±0.740	150.9±4.9	1.237±0.012
U-52-14	228	178.9	1.0	0.002	1674.5	0.893±1.750	1.171±0.930	0.893±1.751	1.171±0.930	148.1±6.2	1.261±0.015
U-52-17	356	158.8	0.7	0.002	859.2	0.872±4.007	1.178±0.330	0.872±4.011	1.178±0.330	139.3±10.9	1.264±0.009

[1]All isotopic ratios are activity ratios, unless otherwise specified. All errors are given as 95% confidence intervals. Measured and detritus-corrected activity ratio errors are reported in percent. Age and initial [^{234}U/^{238}U] errors are absolute. Decay constants used are those of Cheng et al. (2000).

WXSM 52 formed in 2 extended episodes, punctuated by a single hiatus. The growth model (Fig. 7) was constructed using a combination of linear interpolation and stepwise linear fit methods. The dated speleothem began growing during MIS 6 at ~150 ka, ceased growing from ~141 to 118 ka, then resumed growth until ~105 ka, when growth ended. In constructing this growth model, we rejected the youngest sample, U-52-1, due to a very high [^{230}Th/^{238}U] uncertainty. The average growth rate of WXSM 52 was 1.5 cm/ka for MIS 5c–5d, and 3.5 cm/ka for MIS 6. Accordingly, the mean resolution of the stable isotope record from WXSM 52 is 50 years during MIS 5c–5d, and about 25 years during MIS 6. Due to the larger uncertainties in the U–Th ages and, hence, the growth models for the older parts of both stalagmites, we will mainly focus on the paleoclimatic records obtained from the speleothem calcite that grew during MIS 5a, 5b, 5c, and 5d.

5.3. Stable isotopes

The WXSM 51 oxygen isotope record is shown in Fig. 8, a plot of δ^{18}O versus distance from the top of the

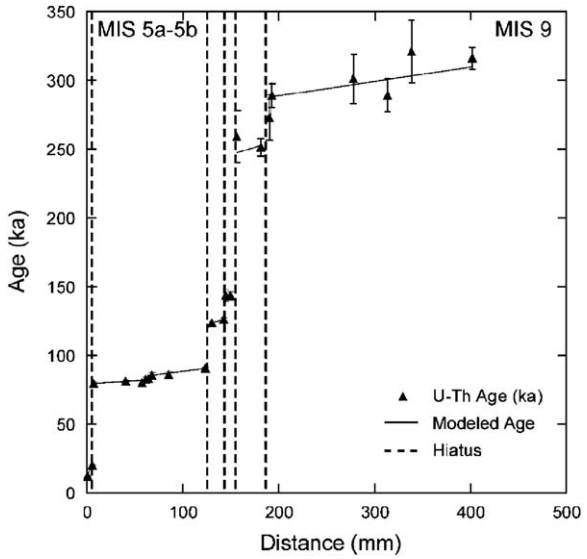

Fig. 6. A plot of U–Th age versus distance for sample WXSM 51. The vertical lines indicate the 5 major depositional hiatuses. The 2σ error bars are shown, except for the cases where they are smaller than the symbol. The growth model age, based on a stepwise linear fit method, is shown as a solid line.

sample. The depositional hiatuses are indicated by the dashed lines, and the Marine Isotope Stage for each period of growth is shown. Marine Isotope Stage 9 was characterized by relatively stable $\delta^{18}O$ values of around −12‰, followed by a rapid increase in $\delta^{18}O$ of about 3‰. The mean $\delta^{18}O$ for this period of growth is − 11.4‰. $\delta^{18}O$ was relatively stable during MIS 8, with a mean value of −7.74‰. The few measurements during the short MIS 6 and MIS 5e periods of growth have a mean $\delta^{18}O$ of −9.02‰ and −12.76‰, respectively.

The MIS 5a–5b $\delta^{18}O$ record is shown plotted versus age in Fig. 9. From 90.7 to 85.9 ka, $\delta^{18}O$ was relatively stable, varying between −9‰ and −10‰, with a mean $\delta^{18}O$ of − 9.34‰. Beginning at 85.9 ka, $\delta^{18}O$ rapidly decreased by 3–4‰ over a period of 200 years. $\delta^{18}O$ remained relatively stable for the next 6 ka, with a mean $\delta^{18}O$ of −12.27‰. The short period of growth that occurred during MIS 2 (Fig. 8) had a mean $\delta^{18}O$ value of −7.49‰. Superimposed on all of these relatively stable time periods are higher frequency $\delta^{18}O$ variations on the order of 0.5‰ to 1.5‰.

A plot of $\delta^{18}O$ versus age is shown in Fig. 10 for the portion of WXSM 52 that grew during MIS 5c and 5d. From the beginning of the record, $\delta^{18}O$ decreased steadily from around − 6.91‰ at 117.6 ka to a minimum of − 13.50‰ at 106.9 ka. $\delta^{18}O$ increased by about 4‰ over the next thousand years, coincident with the deposition of the detrital rich calcite layer. The MIS 6 period of growth in this sample, which is not shown, is characterized by $\delta^{18}O$ values that range from −9.20‰ to −6.14‰, with a mean $\delta^{18}O$ of − 7.88‰.

6. Discussion

6.1. A simple model for interpreting speleothem $\delta^{18}O$ changes

Assuming that Wanxiang Cave stalagmites were deposited under isotopic equilibrium conditions, as discussed above, the $\delta^{18}O$ of speleothem calcite is a function only of temperature in the cave, which equals the MAT at the surface (Wigley and Brown, 1976), and the $\delta^{18}O$ of drip water (Gascoyne, 1992). Speleothem oxygen isotope records from high latitudes have been widely interpreted in terms of changes in paleotemperature; that is, by combining the temperature-dependence of the calcite water fractionation factor (−0.24‰/°C) with the dependence of $\delta^{18}O$ of precipitation (~0.69‰/°C) on air temperature in these regions (Dansgaard, 1964; Gascoyne, 1992), along with expected changes in $\delta^{18}O$ of ocean water, obtained from the marine oxygen isotope record. In this case, assuming that the cave drip water directly reflects the composition of precipitation, the $\delta^{18}O$ of speleothem calcite should be positively correlated with paleotemperature. Unfortunately, this method is not applicable to low latitude or monsoonal regions, where the temperature dependence of the $\delta^{18}O$ in precipitation

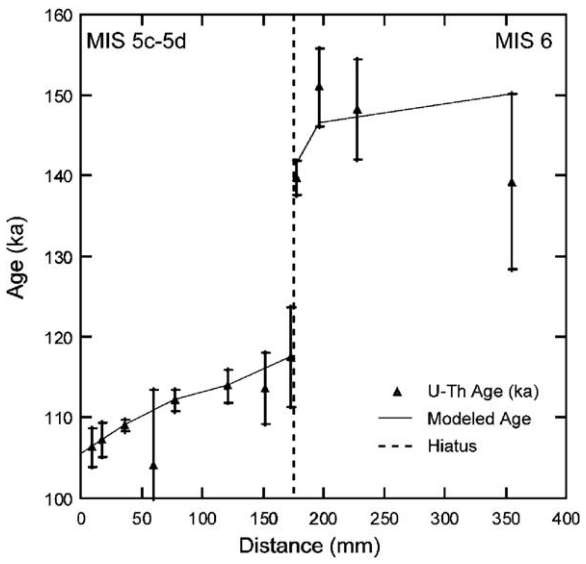

Fig. 7. A plot of U–Th age (with 2σ error bars) versus distance for sample WXSM 52. The vertical line indicates the depositional hiatus. The growth model age, based on a combination of linear regression and stepwise linear fit methods, is shown as a solid line.

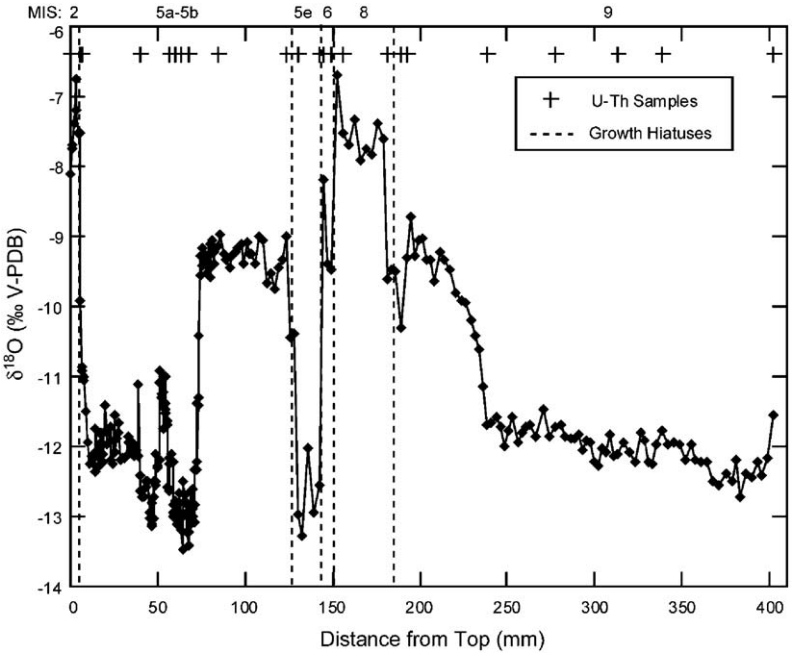

Fig. 8. Oxygen isotopic composition plotted versus distance from the top of the sample for WXSM 51. The depositional hiatuses are indicated by vertical dashed lines. The location of U–Th samples and the Marine Isotope Stage represented by each period of growth are also shown.

is weakened due to the importance of the "amount effect" in these regions; that is, the inverse relationship between $\delta^{18}O$ in precipitation and the amount of precipitation that dominates in regions with convective storm systems (Dansgaard, 1964). Thus, the $\delta^{18}O$ of fossil speleothems collected from Wanxiang Cave, which is near the northern limit of East Asian summer monsoon precipitation in central China, may reflect past changes in temperature and/or precipitation. However, the speleothem $\delta^{18}O$ may also be affected by changes in the summer:winter precipitation (*P*) ratio, changes in source composition due to global ice volume changes, changes in the precipitation:evaporation (*P*:*E*) ratio, and circulation changes. To summarize the possible environmental signals that may be recorded in speleothem $\delta^{18}O$, we constructed a simple schematic model (Fig. 11) to estimate the maximum magnitude of the $\delta^{18}O$ shifts in fossil speleothems that could occur during extreme climate transitions, for example between the LGM, when the East Asian summer monsoon intensity was weak, to the present, when the summer monsoon is relatively strong. Some of the possible effects may be bounded, and appear to be relatively small. For example, a shift of ~2‰ would result from the temperature effect on calcite–water fractionation assuming an 8 °C change from the LGM to present. This is most likely an upper bound on this effect, however, since general circulation models (e.g. CCM1, ECHAM3) predict a LGM-Modern temperature difference of only 3–5° for this region (DKRZ, 1992; Roeckner et al., 1992; Kutzbach et al., 1999). The maximum $\delta^{18}O$ change from global ice volume changes is about 1.5‰ based on the marine oxygen isotope record (Imbrie et al., 1990). We estimate a maximum $\delta^{18}O$ shift of 1‰ due to changes in *P*:*E*, based on studies of evaporation effects in unsaturated zone pore fluids at the Hanford Site, WA (DePaolo et al., 2004; Singleton et al., 2004) In this region, where MAP and net infiltration is much lower than at the Wanxiang Cave site, deep vadose waters are enriched by 2‰ relative to the mean annual precipitation. In a fractured, karst drainage system, infiltration rates are likely higher than at the Hanford site. This combined with approximately three times as much annual precipitation suggests that it is highly unlikely that waters would become significantly enriched prior to infiltration. Also supporting this interpretation are the observations that modern cave waters have an isotopic composition very similar to that of modern precipitation. While we assume that *P*:*E* is lower during the drier, colder periods, it is also possible that the opposite is true. Due to the uncertainty in paleoarchive and GCM *P*:*E* estimates for the LGM in the Asian monsoon region, it is difficult to assess which scenario is true. In either case, this effect is minor and would not significantly change the general pattern of glacial–interglacial $\delta^{18}O$ variability.

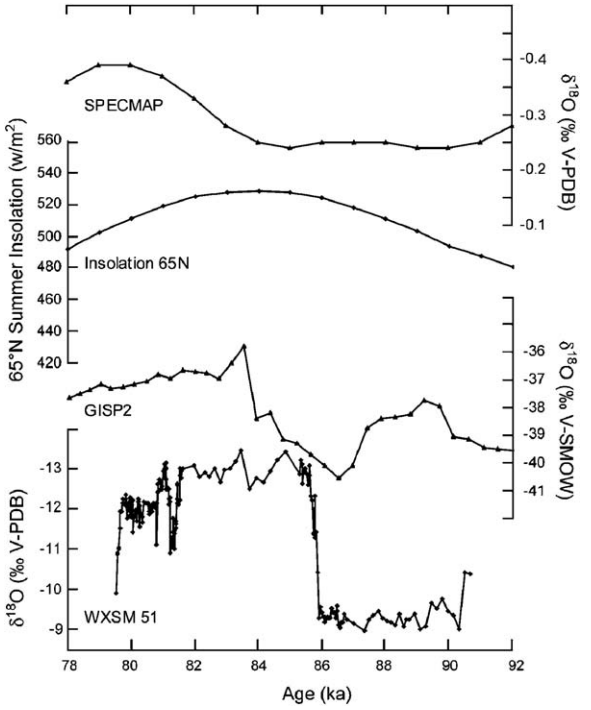

Fig. 9. Oxygen isotopic composition versus age for the MIS 5a–5b section of WXSM 51. Note that the $\delta^{18}O$ scale is reversed to facilitate comparison with other climate records. The 4‰ shift that occurs at approximately 85.7 ka reflects the transition between MIS 5b and MIS 5a, when monsoon intensity increased rapidly over a ~200 year period. Temperatures in Greenland, represented by GISP2 $\delta^{18}O$, increased at about the same time as the shift in monsoon intensity (Grootes and Stuiver, 1997; Petit et al., 1999). Temperatures also increased at Vostok at this time; however, this relationship is less robust. The MIS 5a global ice volume decrease, as represented by the SPECMAP $\delta^{18}O$ curve (Imbrie et al., 1990), appears to lag the increase in monsoon intensity, although they are synchronous within their 2σ errors. Asian monsoon intensity is broadly controlled by Northern Hemisphere summer insolation (e.g. Wang et al., 2001), but the increase in monsoon intensity between MIS 5b and 5a is much more abrupt than the gradually increasing insolation at this time.

The other effects on speleothem $\delta^{18}O$ are more difficult to quantify. The $\delta^{18}O$ of precipitation in central China is controlled both by temperature and by the amount of rainfall (Johnson and Ingram, 2004). The temperature effect on $\delta^{18}O$ of precipitation is the only signal that would be likely to lead to more positive $\delta^{18}O$ values during stronger monsoons. However, in order for this effect to dominate the speleothem $\delta^{18}O$ signal, the $d\delta^{18}O/dT$ slope must be significantly larger than 0.24‰/°C, in order to overcome the negative temperature dependence of the calcite–water fractionation. Assuming a maximum temperature change of 8 °C and a maximum $d\delta^{18}O/dT$ slope of 0.5‰/°C, the largest temperature related shift expected in speleothem $\delta^{18}O$ is 4‰. Again, though, the calcite–water fractionation temperature dependence would counteract that effect, leading to a net change of only around 2‰. Given that both the $d\delta^{18}O/dT$ and the ΔT are likely overestimated in this calculation, the actual net T effect is likely to be much smaller. In fact, Johnson and Ingram (2004) suggest that the temperature dependence of $\delta^{18}O$ in precipitation near the northern limit of the summer monsoon region is not likely to be more than about 0.24‰/°C, in which case T would have no effect at all on speleothem $\delta^{18}O$.

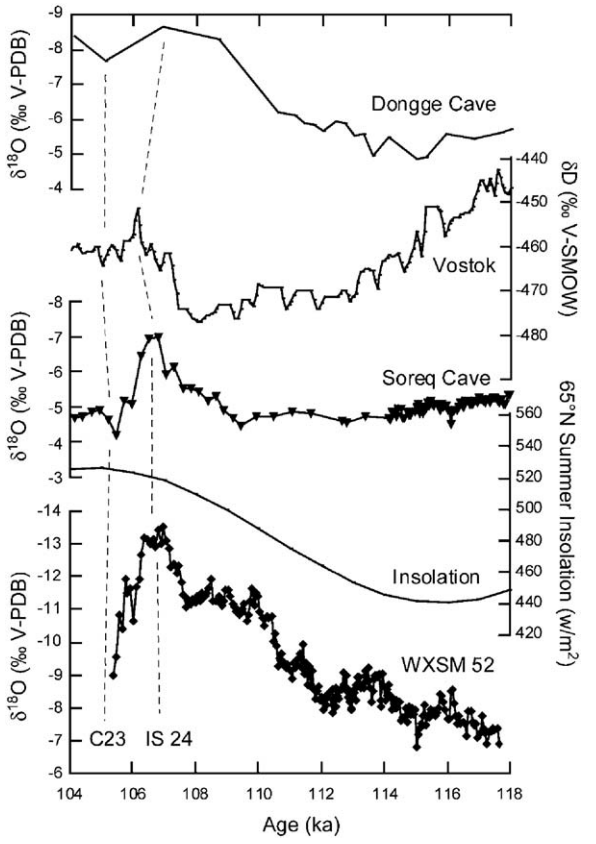

Fig. 10. Oxygen isotopic composition versus age for the MIS 5c–5d section of WXSM 52. Note that the $\delta^{18}O$ scale is reversed to facilitate comparison with other climate records. The Wanxiang Cave record of Asian monsoon intensity shows similarities to the summer insolation at 65°N, the Soreq Cave $\delta^{18}O$ record (Bar-Matthews et al., 2003), Vostok δD (Petit et al., 1999), and the Dongge Cave $\delta^{18}O$ record (Yuan et al., 2004), indicating the strong link between the Asian monsoon and the global climate system. The peak in monsoon intensity at 106.9 ka corresponds to IS 24 and the abrupt decrease following this event may correspond to C23 (McManus et al., 1994). Temperature at Vostok, represented by δD, appears similar to the WXSM 52 record around the time of IS 24 and C23. These events may not have occurred synchronously between the Southern and Northern Hemispheres, though, thus explaining the slight offset in timing.

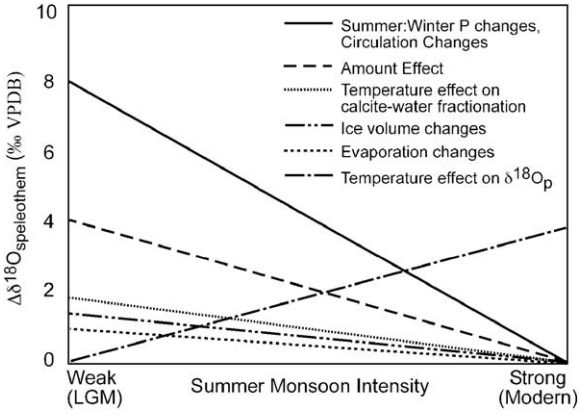

Fig. 11. Schematic model for interpreting $\delta^{18}O$ variations in speleothems from central China. The direction and maximum magnitude of the $\delta^{18}O$ shift that could occur during a shift from a strong summer monsoon (e.g. Modern) to a weak summer monsoon (e.g. LGM) due to related changes in the summer:winter precipitation (P) ratio, atmospheric circulation, the amount of rainfall, global ice volume, evaporation, the temperature effect on calcite–water fractionation, and the temperature effect on the $\delta^{18}O$ of precipitation ($\delta^{18}O_p$).

Changes in the amount effect could potentially lead to a change of 2–3‰. This is based on the partial regression slopes, $\beta_{\log P} = d\delta^{18}O / d\log P$, of mean monthly T, P, and $\delta^{18}O$ data from the Global Network for Isotopes in Precipitation (IAEA/WMO, 2001; Johnson and Ingram, 2004). Assuming a maximum $\beta_{\log P}$ for the Wanxiang Cave region of −4, and a maximum reduction in precipitation of 80%, the largest $\delta^{18}O$ shift that would be recorded in speleothem calcite due to changes in the amount of rainfall is about 3‰. It is unlikely that MAP was reduced by 80‰, however, over any extended time periods, therefore a $\delta^{18}O$ shift of around 1‰ is probably more realistic. We should note, however, that periods of strong summer monsoons are not necessarily characterized by precipitation maxima at every location in the monsoon region. An et al. (2000) reported asynchronous monsoon behavior during the Holocene, with precipitation maxima being closely tied to the position of the monsoon front. Therefore, it is possible that during periods of maximum monsoon intensity, where the monsoon front is at its northernmost position, that precipitation at Wanxiang Cave may not be at its maximum. It is not clear how this would affect the $\delta^{18}O$ of precipitation ($\delta^{18}O_p$,) though, and for this study, we assume that monsoon intensity and amount of precipitation at the study area are closely linked. Changing monsoon intensity could also affect the $\delta^{18}O$ of speleothem calcite by altering the ratio of summer: winter precipitation or changing circulation patterns in such a way that the $\delta^{18}O$ of precipitation is decreased during stronger monsoons. It is difficult to quantify these effects, however, so the 8‰ maximum change was arbitrarily set to reflect the maximum range observed in Wanxiang Cave speleothems.

To summarize the potential interpretations of oxygen isotope records from Wanxiang Cave, all of the factors that affect the $\delta^{18}O$ of speleothem calcite in this region work in the same direction with regard to changing monsoon intensity. Temperature, the only factor that could lead to a shift in the opposite direction, is unlikely to have any significant effects on speleothem $\delta^{18}O$ due to the approximately equal and opposite temperature effect on calcite precipitation. The maximum LGM-Modern difference that could be due purely to the amount effect, ice volume changes, and P:E changes is about 5.5‰. This value is likely a significant overestimate of the actual sum of these effects, and therefore the most likely cause of the large $\delta^{18}O$ range observed in speleothems from Wanxiang Cave are changes in the Summer:Winter P ratio and circulation changes. Of these, however, circulation changes are probably the most significant factor. The seasonal $\delta^{18}O_p$ cycle may be less pronounced at this location than in regions farther south, as similar mean $\delta^{18}O_p$ values during summer and winter are observed at Xian and Chengdu, two nearby GNIP stations. One possible circulation change that may contribute to the decreased $\delta^{18}O$ during stronger monsoons is that a greater fraction of rainfall may be derived from the Indian monsoon system during these periods (An et al., 2000). This would lead to an increase in the distance to the source of rainfall (Indian Ocean or Bay of Bengal), and therefore, a significant depletion in $\delta^{18}O$ of precipitation during strong monsoons.

6.2. The Wanxiang Cave $\delta^{18}O$ records

The results of this schematic model suggest that there will be an inverse relationship between monsoon intensity and the $\delta^{18}O$ of speleothem calcite in samples from Wanxiang Cave. The general pattern of $\delta^{18}O$ variability observed in WXSM 51 (Fig. 8) and WXSM 52 (Fig. 10) support this interpretation. It is well known that, in general, East Asian summer monsoon intensity is decreased during globally cooler periods and increased during warmer periods (Porter, 2001). While speleothem formation seems to occur during both glacial and interglacial periods in this region, the $\delta^{18}O$ signal preserved in speleothem calcite differs somewhat systematically between these two climate states, reflecting these changes in monsoon intensity. The mean $\delta^{18}O$ of speleothem calcite that formed during the stadial episodes, MIS 8, 6, 5d, and 5b, ranges from − 6.91‰ to

9.34‰, while the $\delta^{18}O$ of calcite formed during the interstadial periods, 9, 5e, 5c, and 5a, ranges from −11.9‰ to − 13.5‰ (Figs. 8–10).

The transition between MIS 5d and 5c (Fig. 10) is characterized by a relatively slow, steady decrease in $\delta^{18}O$. The high $\delta^{18}O$ values at 117.6 ka indicate that the monsoon intensity had already returned to a weakened stadial mode by this time, following the Last Interglacial increase in monsoon intensity. Monsoon intensity during this period appears to be related to northern hemisphere insolation suggesting that this external forcing may control the general pattern of monsoon variability. The WXSM 52 record also shows similarities to the Soreq Cave speleothem record (Bar-Matthews et al., 1997; Bar-Matthews et al., 2003), the Vostok *δD* record (Petit et al., 1999), and North Atlantic climate (McManus et al., 1994; Grootes and Stuiver, 1997) during this time.

The Soreq Cave $\delta^{18}O$ signal primarily reflects the amount of precipitation in the Eastern Mediterranean. The rainy season in this region, however, occurs during the winter months of December–May. The minimum $\delta^{18}O$ observed in WXSM 52 during MIS 5c at 106.9 ka indicates a peak in summer monsoon intensity at this time, which corresponds with a peak in winter rainfall at Soreq Cave, as evidenced by the minimum $\delta^{18}O$ of − 6.99‰ at 106.8 ka (Bar-Matthews et al., 2003). This peak in monsoon intensity occurs at the same time as Interstadial 24 (IS 24), observed in the GRIP ice core record, and a period of warm North Atlantic SSTs as documented in the *N. pachyderma* record from marine core V29-191 (Dansgaard et al., 1993; McManus et al., 1994).The abrupt decrease in precipitation that occurred at approximately 106 ka in the Soreq Cave record and in WXSM 52, also corresponds with a North Atlantic surface cooling event, C24 (McManus et al., 1994). Prior to about 109 ka, during MIS 5d, however, the Soreq Cave and Wanxiang Cave records are less similar, as $\delta^{18}O$ in WXSM 52 slowly decreased during this period, the $\delta^{18}O$ at Soreq Cave was relatively stable. A peak in temperature at Vostok, as reflected by *δD*, also occurs around 106 ka, indicating that IS 24 may have been a global event. Again, however, the MIS 5d record from Vostok is less similar, showing decreasing temperatures from 118 to 108 ka.

The WXSM 52 record also closely resembles other records of Asian monsoon variability. The general pattern of $\delta^{18}O$ variability seen in the stalagmite D3 record from Dongge Cave (25°17′ N, 108°50′ E), reported by Yuan et al. (2004), is very similar to the WXSM 52 record for MIS 5d–5c (Fig. 10). IS 24 and C23 also appear as periods of strong and weak monsoon intensity respectively in the D3 record, although the amplitude is lower in the Dongge Cave record. This may be due to the lower sampling resolution of this record (average of ~600 years per sample), or alternatively, may indicate that the $\delta^{18}O$ of precipitation in the Wanxiang Cave region is more sensitive to changes in monsoon intensity, possibly due to its location near the northern limit of the monsoon region, where even small variations in monsoon intensity may have a significant impact on $\delta^{18}O$. Nevertheless, the strong similarity between the two records confirms that Wanxiang Cave speleothem $\delta^{18}O$ preserves a regional climate signal and supports using speleothem $\delta^{18}O$ from the Asian monsoon region as a paleomonsoon proxy. The Chinese Loess record of paleomonsoon intensity also shares many features with the Wanxiang Cave record. Increased magnetic susceptibility and the presence of paleosol S1S2 during MIS 5c, and decreased magnetic susceptibility and the presence of an interbedded loess layer S1L2 during MIS 5d suggests that the summer monsoon intensity was strong during MIS 5c and weak during MIS 5d (Chen et al., 1999). Chen et al. also report that the warm, humid MIS 5c was interrupted by a dusty, colder, and drier period. This may correspond to C23 in WXSM 52 as represented by the abrupt decrease in $\delta^{18}O$ values around 106 ka, the precipitation of detrital rich calcite beginning at this time, and the eventual cessation of speleothem growth.

The transition between MIS 5b and 5a, as recorded in WXSM 51 (Fig. 9) is much more abrupt than the 5d–5c transition. The approximately 4‰ decrease in $\delta^{18}O$ that occurs between 85.9 and 85.6 ka suggests that monsoon intensity increased abruptly during this transition. This increase in monsoon intensity occurs contemporaneously with more gradual warming in Greenland (GISP2). The transition from MIS 5b to 5a in the WXSM 51 record also coincides with a slight warming in Vostok and a decrease in global ice volume as recorded in SPECMAP $\delta^{18}O$ (Imbrie et al., 1990). The increase in monsoon intensity, however, appears to lead the decrease in SPECMAP $\delta^{18}O$ by approximately 4 ka, although this lead is not well resolved considering the uncertainties of the age models of SPECMAP (~4 ka; Martinson et al., 1987) and the WXSM 51 record (~2 ka for this time period).

The transition from a weak summer monsoon during MIS 5b to a strong monsoon during MIS 5a, is also supported by the Chinese Loess record. Magnetic susceptibility was increased and paleosol S1S1 formed during stage 5a, while stage 5b is characterized by decreased magnetic susceptibility and the presence of the interbedded loess layer S1L1 (Chen et al., 1999).

Based on the multi-proxy loess record, Chen et al. suggest that the summer monsoon intensity was stronger during MIS 5c than 5a, and weaker during stage 5b than during stage 5d. While we cannot make any definitive statements about the relative monsoon intensity of these periods, given the fact that the speleothem record does not completely cover all stages, we can make a general statement about relative monsoon intensity for the periods studied. Based purely on the $\delta^{18}O$ signal, it appears that while MIS 5c was characterized by the most negative $\delta^{18}O$ values, representing the most intense summer monsoon of this period, these extreme values were maintained for less than 2000 years. Monsoon intensity during MIS 5a, on the other hand, while never equaling the peak during MIS 5c, was characterized by a more prolonged period of strong summer monsoon precipitation. Likewise, while monsoon intensity increased throughout MIS 5d, reaching minimum $\delta^{18}O$ values of approximately −10‰, the mean $\delta^{18}O$ was actually higher than the mean $\delta^{18}O$ value during MIS 5b, suggesting that the stage 5b summer monsoon was equal to or even stronger than the stage 5d summer monsoon.

7. Conclusions

The $\delta^{18}O$ of speleothems collected from Wanxiang Cave in central China is useful as a qualitative proxy for past changes in East Asian summer monsoon intensity. Periods with increased monsoon intensity are characterized by decreased speleothem $\delta^{18}O$, due to the combination of an increased amount effect, decreased global ice volume, decreased evaporation, an increased summer:winter P ratio, and circulation changes that occur during strong monsoons. Two stalagmites, WXSM 51 and WXSM 52, exhibit generally higher $\delta^{18}O$ during stadial periods (MIS 6, 8, 5d, 5b, and 2) than during interstadial periods (MIS 9, 5a, 5c, 5e), indicating that summer monsoon intensity is generally decreased during globally cooler periods and increased during globally warmer periods.

The close agreement of the MIS 5c–5d record from WXSM 52 and the MIS 5a–5b record from WXSM 51 with global climate records such as the GISP2, Vostok, and SPECMAP records, and the Northern Hemisphere insolation curve, suggest that East Asian summer monsoon intensity varies in phase with global climate fluctuations and is largely controlled by solar insolation in the Northern Hemisphere. The strong similarity between the Wanxiang Cave record and the Soreq Cave $\delta^{18}O$ record suggests that a link may exist between the Asian monsoon and climate in the Eastern Mediterranean region. Climate in both of these regions is strongly dependent on the position and strength of the mid-latitude westerlies. A weakening of the westerlies, which may be linked to changes in North Atlantic Climate or even the North Atlantic Oscillation, could possibly lead to increased precipitation in both the Eastern Mediterranean winter and the East Asian summer.

The MIS 5a–5b and 5c–5d paleomonsoon records from Wanxiang Cave agree well with the Chinese Loess records of Chen et al. (1999), and the speleothem record of Yuan et al. (2004), indicating that $\delta^{18}O$ of speleothems from Wanxiang Cave is a valid proxy for changes in monsoon intensity. The speleothem $\delta^{18}O$ record suggests that the summer monsoon intensity was generally stronger during MIS 5a than 5c and weaker during MIS 5d than 5e.

Acknowledgements

This research was supported by National Geographic Society Grant # 7206-02, NSFC Grant # 40173010, the Esper C. Larsen fund, a Berkeley Geochronology Center Fellowship, and a GSA Graduate Student Research Grant. We thank Kate Trueheart, Doug LaRowe, and Cliff Riebe for their help in the field, and Brendan Roark for valuable discussions and help with the stable isotope analyses.

References

An, Z.S., 2000. The history and variability of the East Asian paleomonsoon climate. Quaternary Science Reviews 19 (1–5), 171–187.

An, Z., Porter, S.C., Kutzbach, J.E., Wu, X., Wang, S., Liu, X., Li, X., Zhou, W., 2000. Asynchronous Holocene optimum of the East Asian monsoon. Quaternary Science Reviews 19 (8), 743–762.

Bar-Matthews, M., Ayalon, A., Kaufman, A., 1997. Late Quaternary paleoclimate in the eastern Mediterranean region from stable isotope analysis of speleothems at Soreq Cave, Israel. Quaternary Research 47, 155–168.

Bar-Matthews, M., Ayalon, A., Gilmour, M., Matthews, A., Hawkesworth, C.J., 2003. Sea-land oxygen isotopic relationships from planktonic foraminifera and speleothems in the eastern Mediterranean region and their implication for paleorainfall during interglacial intervals. Geochimica et Cosmochimica Acta 67 (17), 3181–3199.

Chen, J.H., Edwards, R.L., Wasserburg, G.J., 1986. ^{238}U, ^{234}U, and ^{232}Th in sea water. Earth and Planetary Science Letters 80, 241–251.

Chen, F.H., Bloemendal, J., Feng, Z.D., Wang, J.M., Parker, E., Guo, Z.T., 1999. East Asian monsoon variations during Oxygen Isotope Stage 5: evidence from the northwestern margin of the Chinese loess plateau. Quaternary Science Reviews 18 (8–9), 1127–1135.

Cheng, H., Edwards, R.L., Hoff, J.A., Gallup, C.D., Richards, D.A., Asmerom, Y., 2000. The half-lives of uranium-234 and thorium-230. Chemical Geology 169, 17–33.

COHMAP, 1988. Climatic changes of the last 18,000 years: observations and model simulation. Science 241, 1043–1052.

Dansgaard, W., 1964. Stable isotopes in precipitation. Tellus 16, 436–438.

Dansgaard, W., Johnsen, S.J., Clausen, H.B., Dahl-Jensen, D., Gundestrup, N.S., Hammer, C.U., Hvidberg, C.S., Steffensen, J.P., Sveinbjornsdottir, A.E., Jouzel, J., Bond, G., 1993. Evidence for general instability of past climate from a 250-kyr ice-core record. Nature 364 (6434), 218–220.

DePaolo, D.J., Conrad, M.E., Maher, K., Gee, G.W., 2004. Evaporation effects on oxygen and hydrogen isotopes in deep vadose zone pore fluids at Hanford, Washington. Vadose Zone Journal 3, 220–232.

DKRZ, 1992. The ECHAM3 Atmospheric General Circulation Model, DKRZ Tech. Report. Deutsches Klimarechenzentrum, Hamburg, Germany, p. 184.

Edwards, L., Chen, J.H., Wasserburg, G.J., 1987. ^{238}U–^{234}U–^{230}Th–^{232}Th systematics and the precise measurement of time over the past 500,000 years. Earth and Planetary Science Letters 81, 175–192.

Epstein, J.B., Buchsbaum, R., Lowenstam, H.A., Urey, H.C., 1953. Revised carbonate–water isotopic temperature scale. GSA Bulletin 64, 1315–1326.

Feng, X.H., Cui, H.T., Tang, K.L., Conkey, L.E., 1999. Tree-ring delta D as an indicator of Asian monsoon intensity. Quaternary Research 51 (3), 262–266.

Feng, X.H., Cui, H., Conkey, L.E., 2002. Reply to the letter to the editor by Zhou on "Tree-Ring delta D as an indicator of Asian monsoon intensity". Quaternary Research 58 (2), 212–213.

Fleitmann, D., Burns, S.J., Neff, U., Mangini, A., Matter, A., 2003. Changing moisture sources over the last 330,000 years in northern Oman from fluid-inclusion evidence in speleothems. Quaternary Research 60 (2), 223–232.

Fleitmann, D., Burns, S.J., Neff, U., Mudelsee, M., Mangini, A., Matter, A., 2004. Palaeoclimatic interpretation of high-resolution oxygen isotope profiles derived from annually laminated speleothems from southern Oman. Quaternary Science Reviews 23 (7–8), 935–945.

Gascoyne, M., 1992. Paleoclimate determination from cave calcite deposits. Quaternary Science Reviews 11, 609–632.

Gasse, F., Arnold, M., Fontes, J.C., Fort, M., Gilbert, E., Huc, A., Li, B., Li, Y., Liu, Q., Melieres, F., Van Campo, E., Wang, F., Zhan, Q., 1991. A 13,000 year climate record from western Tibet. Nature 353, 742–745.

Grootes, P.M., Stuiver, M., 1997. Oxygen 18/16 variability in Greenland snow and ice with 10^3- to 10^5-year time resolution. Journal of Geophysical Research-Oceans 102 (C12), 26455–26470.

Hendy, C.H., 1971. The isotopic geochemistry of speleothems: 1. The calculation of the effects of different modes of formation on the isotopic composition of speleothems and their applicability as paleoclimatic indicators. Geochimica et Cosmochimica Acta 35, 801–824.

IAEA/WMO, 2001. Global Network of Isotopes in Precipitation. The GNIP Database.

Imbrie, J. et al., 1990. SPECMAP Archive #1, NOAA/NGDC Paleoclimatology Program, Boulder, CO.

Johnson, K.R., Ingram, B.L., 2004. Spatial and temporal variability in the stable isotope systematics of modern precipitation in China: implications for paleoclimate reconstructions. Earth and Planetary Science Letters 220 (3–4), 365–377.

Kutzbach, J.E., Guetter, P.J., 1986. The influence of changing orbital parameters and surface boundary-conditions on climate simulations for the past 18000 years. Journal of the Atmospheric Sciences 43 (16), 1726–1759.

Kutzbach, J., Guetter, P.J., Behling, P.J., Selinm, R., 1992. Simulated climatic changes: results of the COHMAP climate-model experiments. In: Wright Jr., H.E., et al. (Ed.), Global Climates Since the Last Glacial Maximum. Univ. Minnesota Press, Minneapolis, pp. 24–93.

Kutzbach, J., Gallimore, R., Harrison, S., Behling, P., Selin, R., Laarif, F., 1999. Climate and biome simulations for the past 21,000 years (vol 17, pg 471, 1998). Quaternary Science Reviews, 18(3): I-I.

Ludwig, K.R., 1999. Using Isoplot/Ex: Version 2.01: a geochronological toolkit for Microsoft Excel. Berkeley Geochronology Center Special Publication, vol. 1a, p. 47.

Ludwig, K.R., Paces, J.B., 2002. Uranium-series dating of pedogenic silica and carbonate, Crater Flat, Nevada. Geochimica et Cosmochimica Acta 66 (3), 487–506.

Martinson, D.G., Pisias, N.G., Hays, J.D., Imbrie, J., Moore, T.C., Shackleton, N.J., 1987. Age dating and the orbital theory of the ice ages—development of a high-resolution 0 to 300,000-year chronostratigraphy. Quaternary Research 27 (1), 1–29.

Mccrea, J.M., 1950. On the isotopic chemistry of carbonates and a paleotemperature scale. Journal of Chemical Physics 18 (6), 849–857.

McManus, J.F., Bond, G., Broecker, W.S., Johnsen, S., Labeyrie, L., Higgins, S.M., 1994. High-resolution climate records from the North Atlantic during the last interglacial. Nature 371, 326–329.

Neff, U., Burns, S.J., Mangini, A., Mudelsee, M., Fleitmann, D., Matter, A., 2001. Strong coherence between solar variability and the monsoon in Oman between 9 and 6 kyr ago. Nature 411 (6835), 290–293.

O'Neil, J.R., 1969. Oxygen isotope fractionation in divalent metal carbonates. Journal of Chemical Physics 51, 5547–5558.

Petit, J.R., Jouzel, J., Raynaud, D., Barkov, N.I., Barnola, J.M., Basile, I., Bender, M., Chappellaz, J., Davis, M., Delaygue, G., Delmotte, M., Kotlyakov, V.M., Legrand, M., Lipenkov, V.Y., Lorius, C., Pepin, L., Ritz, C., Saltzmann, E., Stievenard, M., 1999. Climate and atmospheric history of the past 420,000 years from the Vostok ice core Antarctica. Nature 399 (6735), 429–436.

Porter, S.C., 2001. Chinese loess record of monsoon climate during the last glacial–interglacial cycle. Earth-Science Reviews 54 (1–3), 115–128.

Roeckner, E., Arpe, K., Bengtsson, L., Brinkop, S., Duemenil, L., Esch, M., Kirk, E., Lunkeit, F., Ponater, M., Rockel, B., Sausen, R., Schlese, U., Schubert, S., Windelband, M., 1992. Simulation of the Present-Day Climate with the ECHAM Model: Impact of Model Physics and Resolution. 93. Max-Planck-Institut fuer Meteorologie, Hamburg, Germany.

Singleton, M.J., Sonnenthal, E.L., Conrad, M.E., DePaolo, D.J., Gee, G.W., 2004. Multiphase reactive transport modeling of stable isotope fractionation in unsaturated zone pore water and vapor: application to seasonal infiltration events at the Hanford Site, WA. Vadose Zone Journal 3, 775–785.

Sun, X.J., Luo, Y.L., Huang, F., Tian, J., Wang, P.X., 2003. Deep-sea pollen from the South China Sea: Pleistocene indicators of East Asian monsoon. Marine Geology 201 (1–3), 97–118.

Thompson, L.G., Mosley-Thompson, E., Davis, M.E., Bolzan, J.F., Dai, J., Yao, T., Gundestrup, N., Wu, X., Klein, L., Xie, Z., 1989. Holocene–late Pleistocene climatic ice core records from Qinghai–Tibetan Plateau. Science 246, 474–477.

Thompson, L.G., Yao, T., Davis, M.E., Henderson, K.A., Mosley-Thompson, E., Lin, P.N., Beer, J., Synal, H.A., Cole-Dai, J.,

Bolzan, J.F., 1997. Tropical climate instability: the last glacial cycle from a Qinghai–Tibetan ice core. Science 276, 1821–1825.

Thompson, L.G., Yao, T., Mosley-Thompson, E., Davis, M.E., Henderson, K.A., Lin, P.N., 2000. A high-resolution millennial record of the South Asian monsoon from Himalayan ice cores. Science 289 (5486), 1916–1919.

Wang, L., Sarnthein, M., Pflaumann, U., Heilig, S., Kienast, M., Ivanova, E., Erlenkeuser, H., Grootes, P., Grimalt, J.O., Pelejero, C., 1999. East Asian monsoon climate during the late Pleistocene; high-resolution sediment records from the South China Sea. In: Sarnthein, M., Wang, P. (Eds.), Response of West Pacific Marginal Seas to Global Climate Change. Elsevier, Amsterdam, pp. 245–284.

Wang, Y.J., Cheng, H., Edwards, R.L., An, Z.S., Wu, J.Y., Shen, C.C., Dorale, J.A., 2001. A high-resolution absolute-dated late Pleistocene monsoon record from Hulu Cave, China. Science 294, 2345–2348.

Wang, P.X., Jian, Z.M., Zhao, Q.H., Li, Q.Y., Wang, R.J., Liu, Z.F., Wu, G.X., Shao, L., Wang, J.L., Huang, B.Q., Fang, D.Y., Tian, J., Li, J.R., Li, X.H., Wei, G.J., Sun, X.J., Luo, Y.L., Su, X., Mao, S.Z., Chen, M.H., 2003. Evolution of the South China Sea and monsoon history revealed in deep-sea records. Chinese Science Bulletin 48 (23), 2549–2561.

Webster, T.M.L., Magana, V.O., Palmer, T.N., Shukla, J., Tomas, R.A., Yanai, M., Yasunari, T., 1998. Monsoons: processes, predictability, and the prospects for prediction. Journal of Geophysical Research 103, 14,451–14,510.

Wigley, T.M.L., Brown, M.C., 1976. The physics of caves. In: Ford, T.D., Cullingford, C.H.D. (Eds.), The Science of Speleology. Academic Press, London, pp. 329–358.

Yuan, D.X., Cheng, H., Edwards, R.L., Dykoski, C.A., Kelly, M.J., Zhang, M.L., Qing, J.M., Lin, Y.S., Wang, Y.J., Wu, J.Y., Dorale, J.A., An, Z.S., Cai, Y.J., 2004. Timing, duration, and transitions of the last interglacial Asian monsoon. Science 304 (5670), 575–578.

Zhang, P., Johnson, K.R., Chen, Y., Chen, F., Ingram, B.L., Zhang, X., Zhang, C., Wang, S., Pang, F., Long, L., 2004. Modern systematics and environmental significance of stable isotopic variations in Wanxiang Cave, Wudu, Gansu, China. Chinese Science Bulletin 49 (15), 1649–1652.

Zhao, J.X., Wang, Y.J., Collerson, K.D., Gagan, M.K., 2003. Speleothem U-series dating of semi-synchronous climate oscillations during the last deglaciation. Earth and Planetary Science Letters 216 (1–2), 155–161.

Zhou, H.Y., 2002. Comment on “Tree-Ring delta D as an indicator of Asian monsoon intensity”. Quaternary Research 58 (2), 210–211.

Zhou, W., Head, M.J., Lu, X., An, Z., Jull, A.J.T., Donahue, D., 1999. Teleconnection of climatic events between East Asia and polar high latitude areas during the last deglaciation. Palaeogeography, Palaeoclimatology, Palaeoecology 152 (1–2), 163–172.